Acta Astronautica 102 (2014) 47–61

Contents lists available at ScienceDirect

Acta Astronautica

journal homepage: www.elsevier.com/locate/actaastro

Analytical guidance for spacecraft relative motion under constant thrust using relative orbit elements

Riccardo Bevilacqua [a,*], Thomas Alan Lovell [b]

[a] Mechanical, Aerospace, and Nuclear Engineering Department, Rensselaer Polytechnic Institute, 110 8th street, Troy, NY 12180, USA
[b] Research Aerospace Engineer, Air Force Research Laboratory, Space Vehicles Directorate, Kirtland AFB, NM, USA

ARTICLE INFO

Article history:
Received 5 August 2013
Received in revised form
17 April 2014
Accepted 8 May 2014
Available online 15 May 2014

Keywords:
Spacecraft relative motion
On-off thrust
Relative orbit elements
Analytical guidance
Input-shaping

ABSTRACT

Proximity control of modern nano-spacecraft often relies on low and discrete thrust engines that are characterized by low consumption, and generate on-off force profiles. New guidance solutions must take into account the nature of this type of orbital engines. This paper introduces novel analytical guidance solutions for spacecraft relative motion considering continuous, on-off thrust, and using relative orbit elements as a geometrical representation of the dynamics. The solutions provide the relative state vector at any given time, accommodating any thrust magnitude along the three directions of the relative frame, as well as generic activation times and durations. Relative orbit elements geometrically interpret key aspects of the relative motion, including for example, the relative ellipse size, and the evolution of its center in time. The new solutions provide the guidance designer with a direct visualization of the thrust effects on the relative motion geometry, offering new possibilities for analytical guidance in the presence of continuous thrust engines, such as low thrust engines on nano-spacecraft. The paper presents the analytical solutions, and tests their effectiveness using a sample thrust profile based on input-shaping, previously developed by one of the authors using classical Cartesian coordinates. The use of relative orbit elements shows substantial benefits and added simplicity with respect to Cartesian-based approaches, holding the promise for straightforward onboard spacecraft implementation. The software developed for this research will be available open source[1], to be used by spacecraft guidance designers as trajectory design tool.

1. Introduction

Small spacecraft flying in tight formations are nowadays replacing larger single satellites, due to their lower cost, the reconfiguration ability, the flexibility to substitute malfunctioning vehicles without aborting the mission, and their inherent redundancy as multi-vehicle systems [1]. On the other hand, solutions such as the CubeSats[2], present a new set of design challenges, mainly related to the vehicles' limited size, power, and computation abilities. Incorporating thrusters and carrying on-board propellant is extremely difficult on nano-spacecraft weighting a few kilograms [2], and such thrusters

* Corresponding author. Tel.: +1 518 276 4274.
E-mail address: bevilr@rpi.edu (R. Bevilacqua).
[1] ⟨http://www.riccardobevilacqua.com/links.html⟩.
[2] http://www.cubesat.org/ (retrieved June 28th, 2012).

http://dx.doi.org/10.1016/j.actaastro.2014.05.004
0094-5765/

Nomenclature

a	orbital semi-major axis
a_e	relative ellipse semi-major axis
$A_{x,y,z,i}$	amplitude of control force at the ith firing in the x, y, or z direction
β	parametric (phase) angle for the planar motion in terms of ROEs
c	reference thrust value (it represents the nominal thrust available on a spacecraft)
$\Delta t_{x,y,z,i}$	duration of the ith firing in the x, y, or z direction
Δt_w	unknown duration in input-shaping profile
e	orbital eccentricity
γ	parametric (phase) angle for the out of plane motion in terms of ROEs
HCW	Hill–Clohessy–Wiltshire
i_{orb}	orbital inclination
J_2	Earth's second zonal harmonic
LVLH	local vertical local horizontal
μ	Earth's gravitational constant
n	orbital angular rate
$N_{x,y,z}$	number of firings in the x, y, or z direction
ν	orbital polar angle
Ω	orbital right ascension of the ascending node (RAAN)
ω_p	orbital argument of perigee
R_{Earth}	mean radius of the Earth
ROEs	relative orbit elements
s	Laplace complex variable
t	time
t^*	unknown time variable in input-shaping profile
x, y, z	Cartesian coordinates in the LVLH frame
x_d, y_d	center of the 2-by-1 relative ellipse (part of the ROEs variables)
X, Y, Z	Laplace transforms of the Cartesian coordinates in the LVLH frame

Further symbols explanation

Subscript 0 refers to initial conditions (at initial epoch time t_0). Subscript f refers to final epoch.

Dot on a variable represents first time derivative. Two dots, second time derivative, etc.

Subscript h indicates coasting solutions to the relative motion dynamics.

operate at one – or just a few – nominal value of force, i.e. they are on-off only. As for the computational capabilities, very simple programs must be designed for the vehicles to be autonomous. Analytical solutions are needed for straightforward online implementation, and to completely avoid the need of onboard numerical iterations.

The relative motion of spacecraft formations is commonly represented in a relative frame using Cartesian coordinates. Relative orbit elements (ROEs) represent a nonlinear transformation from Cartesian coordinates to geometric variables, giving a visual and straightforward understanding of the main aspects of proximity flight dynamics. Other researchers have presented various solutions separating the oscillatory and drifting motions in the classical linearized equations of spacecraft relative motion [3–6], using linear transformations. These previous efforts are not directly and thoroughly addressing the geometrical problem of relative motion. In particular, ROEs are akin to classical orbital elements, in that they consist of physical lengths and angles allowing easy visualization of any relative orbit (a benefit not provided in Refs. [3–6]).

This paper presents the general analytical solution for the time evolution of the ROEs, when on/off constant thrust is used. These results are of particular interest for missions employing low thrust engines. The new solutions also hold the potential for on-board implementation. Alternately, given their analytical nature, they may serve as an initial guess for numerical optimizers to minimize fuel/time, and enable verification of various pre-designed thrust profiles. In this paper the authors demonstrate the last feature, by deriving solutions for orbital planar re-phasing (moving to a new location along track) or rendezvous (moving to the location of a chief satellite, i.e. the origin of the relative motion frame) using thrust profiles based on input-shaping.

Input-shaping has been extensively used in vibration suppression for flexible manipulators Refs. [7–14], but never for orbital control, to the authors' knowledge. Input-shaping is a convolution technique based on the knowledge of a system's natural frequencies of oscillation. Given a feed-forward control signal, designed to perform a desired maneuver, but not taking into account potential excitation of undesired oscillations, input-shaping consists of the convolution of the signal itself and a specified train of impulses, so that the system's resulting behavior presents minimal residual vibrations at the end of the maneuver. The impulses and their locations in time are computed based on the frequencies that need to be suppressed, i.e. the modes one wants to limit in amplitude. The majority of input-shaping applications falls under the category of flexible structures control, such as space manipulators control. It is important to underline that input-shaping is not intended to reduce the energy of a system. Roughly speaking, existing oscillations cannot be damped with input-shaping, while maneuvers from an equilibrium set to a new equilibrium set are possible, as in the case of re-phasing maneuvers. In the specific context of spacecraft relative motion, oscillations refer to periodic motion in the position coordinates.

Exploiting the new analytical formulas, the special case of an input-shaping profile is presented, and the analytical solution for spacecraft planar rendezvous with along-track control only is derived. In addition, the paper demonstrates how the input-shaped control profile can be ad-hoc modified to obtain a final close relative motion of desired size relative to a reference satellite. Sample numerical simulations show some of the maneuvers achieved via the analytical solutions.

The intended advancements in the state of the art for relative motion guidance design are:

- Use of ROEs in conjunction with on-off thrust profiles, thus enabling geometrical visualization of the key aspects of relative motion, and addressing modern engines found especially in small satellites.
- Analytical solutions for ROEs time evolution, and examples of their use with a specific open-loop thrust signal and a closed-loop application.
- Illustration of potential future uses for the new analytical formulas.

The paper is organized as follows. Section 2 presents the spacecraft relative motion dynamics in Cartesian coordinates and its nonlinear transformation in ROEs. Section 3 is dedicated to the derivation of the general analytical equations for the ROEs evolution in time when on-off thrust is used. Section 4 shows the example where an input-shaping-based along-track thrust profile is applied to the new analytical equations, to derive close form guidance solutions for re-phasing maneuvers. Section 5 illustrates the guidance obtained in the previous section with numerical simulations. The same section also presents one closed-loop example where the guidance is computed iteratively when used in a more realistic nonlinear simulation environment. Section 6 draws the conclusions and suggests future applications for the new analytical solutions. The software developed in Matlab® and Simulink® for this investigation will be made available open source (link in Ref. [15]), for interested researchers and guidance designers.

2. Satellite relative dynamics

Consider two satellites orbiting in close proximity to each other. For this analysis, one will be referred to as the reference satellite, or "chief," and the other as the "deputy." For the methods presented here, it is assumed that the only force acting on each satellite is that of a point mass gravitational field, the chief is in a circular orbit, and the distance between the satellites is small compared to their orbital radius. These assumptions yield the following linear time-invariant differential equations [16,17]:

$$\begin{aligned}&\ddot{x}-2n\dot{y}-3n^2x=0\\&\ddot{y}+2n\dot{x}=0\\&\ddot{z}+n^2z=0\end{aligned}\tag{1}$$

These are known as the Hill–Clohessy–Wiltshire (HCW) equations and are written in the local-vertical, local-horizontal (LVLH) coordinate frame, whose origin is at the chief satellite. In these equations, x is the component of the deputy's position vector relative to the chief in the radial direction positive away from the Earth, y is the along-track component positive along the velocity vector of the chief, and z is the cross-track component perpendicular to the orbital plane of the chief. n is the mean motion of the chief. The LVLH frame is depicted in Fig. 1.

The solution to Eq. (1) is:

$$\begin{aligned}x&=\frac{\dot{x}_0}{n}\sin(nt)-\left(3x_0+\frac{2\dot{y}_0}{n}\right)\cos(nt)+\left(4x_0+\frac{2\dot{y}_0}{n}\right)\\y&=\frac{2\dot{x}_0}{n}\cos(nt)+\left(6x_0+\frac{4\dot{y}_0}{n}\right)\sin(nt)-(6nx_0+3\dot{y}_0)t-\frac{2\dot{x}_0}{n}+y_0\\z&=\frac{\dot{z}_0}{n}\sin(nt)+z_0\cos(nt)\\\dot{x}&=\dot{x}_0\cos(nt)+(3nx_0+2\dot{y}_0)\sin(nt)\\\dot{y}&=-2\dot{x}_0\sin(nt)+(6nx_0+4\dot{y}_0)\cos(nt)-(6nx_0+3\dot{y}_0)\\\dot{z}&=\dot{z}_0\cos(nt)-nz_0\sin(nt)\end{aligned}\tag{2}$$

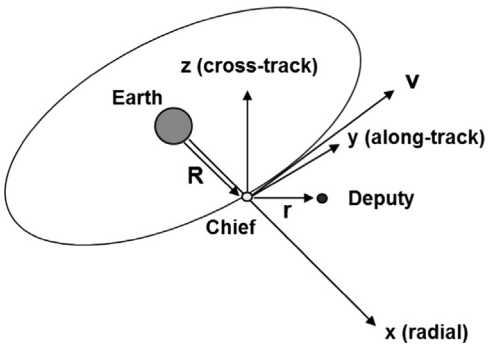

Fig. 1. Depiction of LVLH Frame.

where x_0, y_0, etc, are conditions at some epoch time t_0, and t is the time since t_0. Consider the following change of coordinates from $x, y, z, \dot{x}, \dot{y}, \dot{z}$ [18]:

$$a_e = 2\sqrt{\left(\frac{\dot{x}}{n}\right)^2 + \left(3x + 2\frac{\dot{y}}{n}\right)^2} \quad x_d = 4x + 2\frac{\dot{y}}{n}$$

$$y_d = y - 2\frac{\dot{x}}{n}\beta = \text{atan2}(\dot{x}, 3nx + 2\dot{y})$$

$$z_{\max} = \sqrt{\left(\frac{\dot{z}}{n}\right)^2 + z^2}\gamma = \text{atan2}(nz, \dot{z}) - \text{atan2}(\dot{x}, 3nx + 2\dot{y}) \tag{3}$$

where a_e, x_d, y_d, β, $z_{\max}$, and γ are the ROEs. The inverse of this transformation is

$$x = \frac{-a_e}{2}\cos\beta + x_d \quad \dot{x} = \frac{a_e}{2}n\sin\beta$$

$$y = a_e\sin\beta + y_d \quad \dot{y} = a_e n\cos\beta - \frac{3}{2}nx_d$$

$$z = z_{\max}\sin(\gamma+\beta) \quad \dot{z} = z_{\max} n\cos(\gamma+\beta) \tag{4}$$

It has been shown in Ref. [18] how the ROEs evolve with time:

$$\begin{aligned} a_e &= a_{e0} & x_d &= x_{d0} \\ y_d &= y_{d0} - \tfrac{3}{2}nx_{d0}t = y_{d0} - \tfrac{3}{2}nx_d t & \beta &= \beta_0 + nt \\ z_{\max} &= z_{\max\,0} & \gamma &= \gamma_0 \end{aligned} \tag{5}$$

These equations are analogous to Eq. (2) for $x, y, z, \dot{x}, \dot{y}, \dot{z}$ in that they express the ROEs values at any given time as a function of their initial (epoch) values and the time since epoch.

The parameterization of Eq. (4) reveals that the relative motion of the deputy with respect to the chief in the $\underline{x}$–y plane is a superposition of periodic motion in x and y, with period equal to that of the chief's orbit, and secular motion in y. Essentially, this is an elliptical path that is drifting in the y-direction at a rate of $-3/2nx_d$. The instantaneous center of the ellipse is (x_d, y_d). It has a semi-major axis of length a_e in the along-track direction and semi-minor axis of length $a_e/2$ in the radial direction. β is a parametric angle (i.e. phase angle) indicating the location of the deputy satellite in its trajectory, with $\beta=0$ corresponding to the perigee location (the "bottom" of the ellipse). The relative motion in x and y, if the elliptical path were "frozen" at a point in time, is depicted in Fig. 2. Although the ellipse is actually drifting, it has been frozen in order to conveniently label the ROEs. The z-component of the relative motion, according to the HCW model, is purely sinusoidal and independent of x and y. This motion is a simple harmonic oscillator with amplitude $z_{\max}$ and phase angle $\gamma+\beta$. The deputy intersects the chief's orbit plane at $\gamma+\beta=0$ and π, and reaches $z_{\max}$ and $-z_{\max}$ at $\gamma+\beta=\pi/2$ and $3\pi/2$, respectively. Thus, γ represents the phase difference between the x and y motion and the z motion. Fig. 3 depicts a typical 3-D relative trajectory, with $z_{\max}$ and γ labeled. (NOTE: Because β and γ are angular representations of time – similar to mean anomaly – they are labeled in Figs. 2 and 3 as $\beta^*$and γ^*, which are the physical interpretations of these angles.)

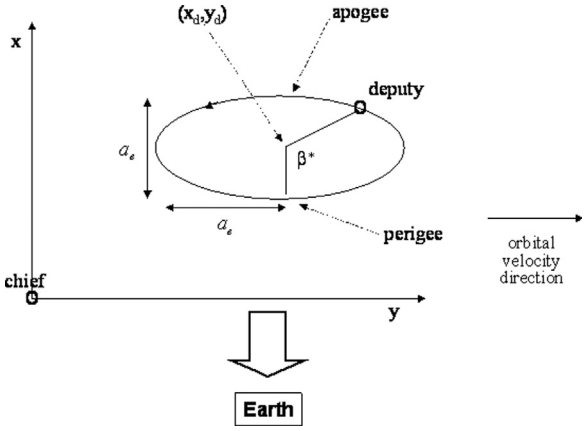

Fig. 2. Planar projection of relative motion trajectory with relative orbit elements labeled.

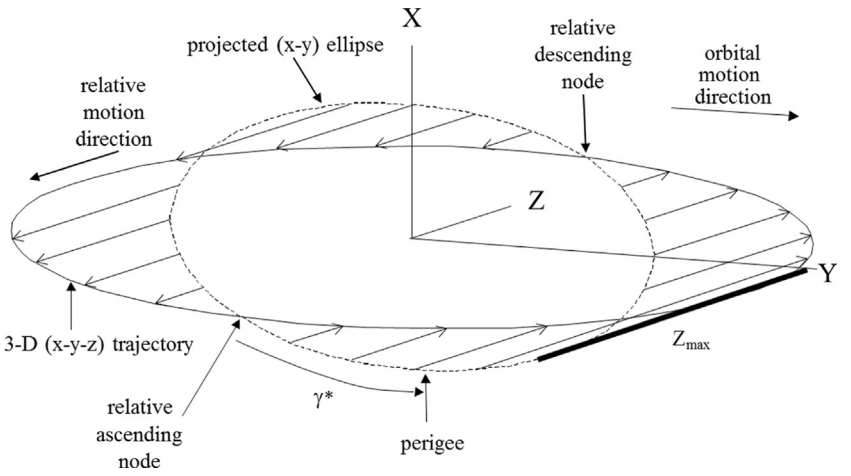

Fig. 3. Depiction of out-of-plane relative motion with relative orbit elements labeled.

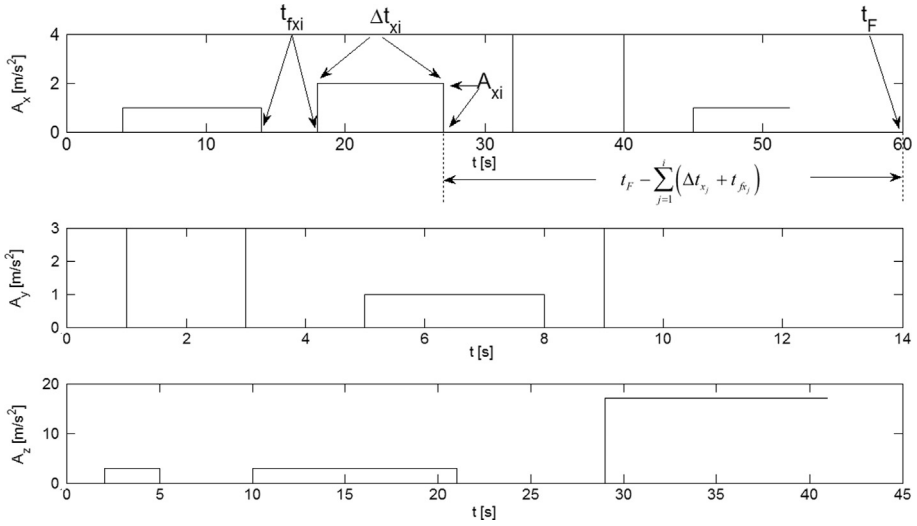

Fig. 4. Generic example of on-off continuous thrust profile.

3. Analytical solutions with continuous on-off thrust

This section presents the steps to derive the closed-form solutions for the time evolution of the ROEs when a generic on-off, continuous thrust profile is assumed in each direction of the LVLH reference frame. $A_{x,y,z,i}$ indicates the magnitude of the ith firing in the x, y, or z direction. $\Delta t_{x,y,z,i}$ is the corresponding time duration of the firing, while $t_{f_{x,y,z,i}}$ is the coasting (off) time duration between the $(i-1)$th and the ith firing. t_F is the final time (see Fig. 4). Note that, if the first firing in a particular direction begins at $t=0$, then t_{f_1} in that direction is defined to be 0.

Because the dynamics we started from are linear (Eq. (1)), the superposition principle can be applied to find the state at the final time. In particular, the final state can be written as the sum of the value at the final time when coasting from the initial condition, plus each of the final values obtained by starting at zero initial conditions, coasting for a duration equal to $\sum_1^{i-1}\left(t_{f_j}+\Delta t_j\right)+t_{f_i}$, applying the generic ith thrust for its given duration, and then coasting for a duration equal to $t_F-\sum_{j=1}^{i}\left(\Delta t_j+t_{f_j}\right)$. In the previous expressions the subscript indicating the direction of the firing was removed, indicating its validity for any axis. For each of the x, y, and z components, the ROEs offer a simple solution, since coasting from a set of

initial conditions is represented by the equations:

$$\begin{aligned} a_e &= a_{e0} \\ x_d &= x_{d0} \\ y_d &= y_{d0} - \tfrac{3}{2} n x_{d0} t_F \\ \beta &= \beta_0 + n t_F \\ z_{\max} &= z_{\max\,0} \\ \gamma &= \gamma_0 \end{aligned} \tag{6}$$

Finding the final state after firing from zero initial conditions, and then coasting, requires the combination of Cartesian coordinates to find the state right after firing, then conversion to ROEs, and finally coasting, using the same form as in Eq. (6). Eq. (11) gives the values of the Cartesian relative states after a generic single firing of duration Δt and coasting period t beforehand, with components in the x, y, and z directions. They can be derived using Laplace transform on the system in Eq. (1), when applying control accelerations $A_{x,y,z,i}$. If s is the Laplace complex variable, we start from:

$$\begin{aligned} &s^2X(s) - sx_0 - \dot{x}_0 - 2n\left[sY(s) - sy_0\right] - 3n^2X(s) = \tfrac{A_x}{s} \\ &s^2Y(s) - sy_0 - \dot{y}_0 + 2n[sX(s) - x_0] = \frac{A_y}{s} \\ &s^2Z(s) - sz_0 - \dot{z}_0 + n^2Z(s) = \frac{A_z}{s} \end{aligned} \tag{7}$$

Solving Eq. (7) in the Laplace domain we obtain:

$$\begin{aligned} \begin{bmatrix} X(s) \\ Y(s) \end{bmatrix} &= \tfrac{1}{s^2(s^2+n^2)} \begin{bmatrix} s^2 - 3n^2 & -2ns \\ 2ns & s^2 \end{bmatrix} \begin{bmatrix} \frac{A_x}{s} + sx_0 + \dot{x}_0 - 2nsy_0 \\ \frac{A_y}{s} + sy_0 + \dot{y}_0 + 2nx_0 \end{bmatrix} \\ Z(s)(s^2+n^2) &= \tfrac{A_z}{s} + sz_0 + \dot{z}_0 \end{aligned} \tag{8}$$

which further simplifies into:

$$\begin{aligned} X(s) &= X_h(s) + \frac{A_x}{s(s^2+n^2)} + \frac{2nA_y}{s^2(s^2+n^2)} \\ Y(s) &= Y_h(s) + \frac{4A_y}{s(s^2+n^2)} - \frac{2nA_x}{s^2(s^2+n^2)} - \frac{3A_y}{s^3} \\ Z(s) &= \frac{A_z}{s(s^2+n^2)} + Z_h(s) \end{aligned} \tag{9}$$

and finally, converting back in the time domain:

$$\begin{aligned} x &= x_h + \tfrac{A_x}{n^2}[1 - \cos(nt)] + 2\tfrac{A_y}{n}\left[t - \tfrac{\sin(nt)}{n}\right] \\ y &= y_h + 4\frac{A_y}{n^2}[1 - \cos(nt)] - 2\frac{A_x}{n}\left[t - \frac{\sin(nt)}{n}\right] - \frac{3}{2}A_y t^2 \\ z &= z_h + \frac{A_z}{n^2}[1 - \cos(nt)] \\ \dot{x} &= \dot{x}_h + \frac{A_x}{n}\sin(nt) + 2\frac{A_y}{n}[1 - \cos(nt)] \\ \dot{y} &= \dot{y}_h + 4\frac{A_y}{n}\sin(nt) - 2\frac{A_x}{n}[1 - \cos(nt)] - 3A_y t \\ \dot{z} &= \dot{z}_h + \frac{A_z}{n}\sin(nt) \end{aligned} \tag{10}$$

where x_h, y_h, and z_h represent the solution of the HCW equations for unforced motion (i.e. Eq. (2)). To apply the superposition principle described earlier, we only need to retain the portion of Eq. (10) generated by control accelerations, i.e. we consider null initial conditions. This provides Eq. (11).

$$\begin{aligned} x^+ &= \tfrac{A_x}{n^2}[1 - \cos(n\Delta t)] + 2\tfrac{A_y}{n}\left[t - \tfrac{\sin(n\Delta t)}{n}\right] \\ y^+ &= 4\frac{A_y}{n^2}[1 - \cos(n\Delta t)] - 2\frac{A_x}{n}\left[t - \frac{\sin(n\Delta t)}{n}\right] - \frac{3}{2}A_y t^2 \\ z^+ &= \frac{A_z}{n^2}[1 - \cos(n\Delta t)] \end{aligned}$$

$$\dot{x}^+ = \frac{A_x}{n}\sin(n\Delta t) + 2\frac{A_y}{n}[1-\cos(n\Delta t)]$$

$$\dot{y}^+ = 4\frac{A_y}{n}\sin(n\Delta t) - 2\frac{A_x}{n}[1-\cos(n\Delta t)] - 3A_y\Delta t$$

$$\dot{z}^+ = \frac{A_z}{n}\sin(n\Delta t) \tag{11}$$

Eq. (3) is then used to convert the Cartesian relative states (Eq. (11)) into ROEs, and the ROEs are propagated for the coasting period according to Eq. (6). This is repeated for each single firing, with N_x, N_y, N_z indicating the total number of firings along each axis. By adding together all the states obtained as described above, the following closed-form solutions for the ROEs subject to generic thrust profiles are obtained:

$$a_e(t_F) = 2\sqrt{\begin{pmatrix}(a_{e_0}/2)\sin(\beta_0+nt_F)\\ -\sum_{i=1}^{N_x}\sqrt{-(2/n^4)A_{x_i}^2(-1+\cos(n\Delta t_{x_i}))}\sin\left(-\beta_{x_i}^+ - n\left(t_F-\sum_{j=1}^{i}(\Delta t_{x_j}+t_{fx_j})\right)\right)\\ +2\sum_{i=1}^{N_y}\sqrt{-(2/n^4)A_{y_i}^2(-1+\cos(n\Delta t_{y_i}))}\sin\left(\beta_{y_i}^+ + n\left(t_F-\sum_{j=1}^{i}(\Delta t_{y_j}+t_{fy_j})\right)\right)\end{pmatrix}^2 + \begin{pmatrix}(a_{e_0}/2)\cos(\beta_0+nt_F)\\ -\sum_{i=1}^{N_x}\sqrt{-(2/n^4)A_{x_i}^2(-1+\cos(n\Delta t_{x_i}))}\cos\left(-\beta_{x_i}^+ - n\left(t_F-\sum_{j=1}^{i}(\Delta t_{x_j}+t_{fx_j})\right)\right)\\ +2\sum_{i=1}^{N_y}\sqrt{-(2/n^4)A_{y_i}^2(-1+\cos(n\Delta t_{y_i}))}\cos\left(\beta_{y_i}^+ + n\left(t_F-\sum_{j=1}^{i}(\Delta t_{y_j}+t_{fy_j})\right)\right)\end{pmatrix}^2} \tag{12a}$$

$$\beta_{x_i}^+ = \mathrm{atan2}((A_{x_i}/n)\sin(n\Delta t_{x_i}), -(A_{x_i}/n)(1-\cos(n\Delta t_{x_i})))$$
$$\beta_{y_i}^+ = \mathrm{atan2}((2A_{y_i}/n)(1-\cos(n\Delta t_{y_i})), (2A_{y_i}/n)\sin(n\Delta t_{y_i}))$$

$$x_d(t_F) = x_{d_0} + \left(\frac{2}{n}\right)\sum_{i=1}^{N_y}A_{y_i}\Delta t_{y_i}$$

$$y_d(t_F) = y_{d_0} - \left(\frac{3}{2}\right)nx_{d_0}t_F - \left(\frac{2}{n}\right)\sum_{i=1}^{N_x}A_{x_i}\Delta t_{x_i} - \left(\frac{3}{2}\right)\sum_{i=1}^{N_y}A_{y_i}\Delta t_{y_i}^2$$
$$-3\sum_{i=1}^{N_y}A_{y_i}\Delta t_{y_i}\left(t_F-\sum_{j=1}^{i}\left(\Delta t_{y_j}+t_{fy_j}\right)\right) \tag{12b}$$

$$\beta(t_F) = a\tan 2\left(\begin{pmatrix}(1/2n)\begin{pmatrix}a_{e_0}n^2\cos(\beta_0+nt_F)+\\ \sum_{i=1}^{N_x}2A_{x_i}\sqrt{(2-2\cos(n\Delta t_{x_i}))}\cos\left(-\beta_{x_i}^+ - nt_F + n\sum_{j=1}^{i}(\Delta t_{x_j}+t_{fx_j})\right)+\\ \sum_{i=1}^{N_y}4A_{y_i}\sqrt{(2-2\cos(n\Delta t_{y_i}))}\cos\left(-\beta_{y_i}^+ - nt_F + n\sum_{j=1}^{i}(\Delta t_{y_j}+t_{fy_j})\right)\end{pmatrix}\\ (1/2n)\begin{pmatrix}a_{e_0}n^2\sin(\beta_0+nt_F)-\\ \sum_{i=1}^{N_x}2A_{x_i}\sqrt{(2-2\cos(n\Delta t_{x_i}))}\sin\left(-\beta_{x_i}^+ - nt_F + n\sum_{j=1}^{i}(\Delta t_{x_j}+t_{fx_j})\right)-\\ \sum_{i=1}^{N_y}4A_{y_i}\sqrt{(2-2\cos(n\Delta t_{y_i}))}\sin\left(-\beta_{y_i}^+ - nt_F + n\sum_{j=1}^{i}(\Delta t_{y_j}+t_{fy_j})\right)\end{pmatrix}\end{pmatrix}, \tag{12c}$$

$$\beta_{x_i}^+ = \mathrm{atan2}((A_{x_i}/n)\sin(n\Delta t_{x_i}), -(A_{x_i}/n)(1-\cos(n\Delta t_{x_i})))$$
$$\beta_{y_i}^+ = \mathrm{atan2}((2A_{y_i}/n)(1-\cos(n\Delta t_{y_i})), (2A_{y_i}/n)\sin(n\Delta t_{y_i}))$$

$$z_{\max}(t_F)=\sqrt{\left(\begin{array}{c} z_{\max_0}\ \cos(\gamma_0+\beta_0+nt_F)+ \\ \sum_{i=1}^{Nz}(A_{z_i}/n^2)\sqrt{(2-2\ \cos(n\Delta t_{z_i}))}\ \cos\left(-\psi_i-n\left(t_F-\sum_{j=1}^{i}(\Delta t_{z_j}+t_{fz_j})\right)\right) \end{array}\right)^2+\left(\begin{array}{c} z_{\max_0}\ \sin(\gamma_0+\beta_0+nt_F)- \\ \sum_{i=1}^{Nz}(A_{z_i}/n^2)\sqrt{(2-2\ \cos(n\Delta t_{z_i}))}\ \sin\left(-\psi_i-n\left(t_F-\sum_{j=1}^{i}(\Delta t_{z_j}+t_{fz_j})\right)\right) \end{array}\right)^2}$$

$$\psi_i=\operatorname{atan2}((A_{z_i}/n)(1-\ \cos(n\Delta t_{z_i})),\ (A_{z_i}/n)\sin(n\Delta t_{z_i}) \tag{12d}$$

$$\gamma(t_F)=\operatorname{atan2}\left(\begin{array}{l} nz_{\max_0}\ \sin(\gamma_0+\beta_0+nt_F)- \\ \sum_{i=1}^{N_z}(A_{z_i}/n)\sqrt{2-2\ \cos(n\Delta t_{z_i})}\ \sin\left(-\psi_i-n\left(t_F-\sum_{j=1}^{i}(\Delta t_{z_j}+t_{fz_j})\right)\right), \\ nz_{\max_0}\ \cos(\gamma_0+\beta_0+nt_F)+ \\ \sum_{i=1}^{N_z}(A_{z_i}/n)\sqrt{2-2\ \cos(n\Delta t_{z_i})}\ \cos\left(-\psi_i-n\left(t_F-\sum_{j=1}^{i}(\Delta t_{z_j}+t_{fz_j})\right)\right) \end{array}\right)-\beta(t_F)$$

$$\psi_i=\operatorname{atan2}((A_{z_i}/n)(1-\ \cos(n\Delta t_{z_i})),\ (A_{z_i}/n)\sin(n\Delta t_{z_i}))$$

Eqs. (12a)–(12d) were obtained through a combination of symbolic calculation and numerical verification in Matlab®. Roughly speaking, each firing, i.e. each non zero phase in the example of Fig. 4 corresponds to one instance of Eq. (11), its transformation into ROEs (Eq. (3)), followed by coasting until final time (Eq. (6)). The difference between each firing is represented by its duration (Δt in Eq. (11)) and the time remaining to reach final time (t_F in Eq. (6) becomes $t_F-\sum_{j=1}^{i}(\Delta t_j+t_{f_j})$, with the i and j indexes explained earlier in this section. The use of software tools enabled compact formulation of the final analytical solutions (12a)–(12d), and the scripts used to obtain and validate them will be available open source.

Despite their complicated appearance, Eqs. (12a)–(12d) represent a powerful tool for trajectory design, since they are analytical and because they heavily simplify for specific applications. The input-shaping example in the following section shows one such simplification, and in general, real spacecraft applications may reduce the number of variables in (12a)–(12d), for example having only one value of thrust, or fixed durations of the firings, etc.

4. Example of planar application of the roe formulas: Input-shaping thrust profile

In this section a validation of some of Eqs. (12a)–(12d) is performed. In particular, one of the results previously obtained by one of the authors using Cartesian coordinates Ref. [19] is confirmed by means of ROEs, obtaining a simpler expression. In Ref. [19], an input-shaping-based, y-only thrust profile was proved to be an effective means to obtain analytical leader-follower re-phasing or rendezvous guidance, as well as equilibrium-relative-orbit to equilibrium-relative-orbit guidance. Such a profile allows for in-plane control, moving the center of the ellipse to a new desired location, where the ellipse collapses to a point for leader-follower maneuvers. The thrust profile was presented in Ref. [19] as follows: (12a)

$$\begin{array}{llll} A_{x_i}=A_{z_i}=0 & u=c\times\operatorname{sign}(y_{d_0}-y_{d_f}), & c>0 & t_F=3t^*+2\Delta t_w \\ A_{1,2,5,6}=\pm\frac{1}{4}u, & t_{f_{1,2,4,6}}=0, & & \Delta t_{1,\ldots,6}=\frac{t^*}{2} \\ A_{3,4}=\pm\frac{1}{2}u, & t_{f_{3,5}}=\Delta t_w & & \end{array} \tag{13}$$

Section 5 shows the typical shape of the input-shaping profiles. Representative experiments showing how input-shaping can be applied, for example, to bang–bang control profiles can be seen in the video in Ref. [20]. The profile of Eq. (13) consists of known amplitudes for the firings (c is a given control amplitude), while the Δt_w and t^* are to be determined. y_{d_0} and y_{d_f} are the initial and final (desired) along track positions of the relative ellipse's center, respectively. Substituting Eq. (13) into Eq. (12b) and assuming $y_{d_0}>y_{d_f}$, the following expressions are obtained:

$$\begin{aligned} x_d(t_F)&=x_{d_0} \\ y_d(t_F)&=y_{d_0}-\left(\frac{3}{4}\right)c(t^*)^2 \end{aligned} \tag{14}$$

Eq. (14) leads to the solution for t^*, given initial and desired final values for y_d, that is, initial and final centers of the ellipse of relative motion.

$$t^*=\sqrt{4\frac{y_{d_0}-y_d(t_F)}{3u}} \tag{15}$$

Note that this result is not as straightforward to find in Cartesian coordinates (Ref. [19]), in which case there is also no geometrical interpretation.

Substitution of the profile of Eq. (13) in Eq. (12a) does not lead to an expression of comparable simplicity. Nevertheless, several observations can be made that provide useful insight with regards to the expected final value for a_e. First of all, all the terms where thrust along x appears are zero. Secondly, the terms not containing a_{e_0} in Eq. (12a), in the square powers, represent modifications with respect to the initial value of a_e. In fact, if no thrusting was present, the final value for a_e would be a_{e_0}, as expected. These observations justify focusing on only some of the resulting terms in Eq. (12a), and specifically we here analyze the following portion, where the square power is omitted for simplicity:

$$2\sum_{i=1}^{N_y}\sqrt{-\left(\frac{2}{n^4}\right)A_{y_i}^2\left(-1+\cos\left(n\Delta t_{y_i}\right)\right)}\sin\left(\beta_{y_i}^{+}+n\left(t_F-\sum_{j=1}^{i}\left(\Delta t_{y_j}+t_{fy_j}\right)\right)\right) \tag{16}$$

After some algebra, and the use of Prosthaphaeresis formulas, Eq. (16) becomes:

$$\frac{1}{2}\sqrt{\frac{2u^2}{n^4}\left(1-\cos\left(n\frac{t^*}{2}\right)\right)}\begin{pmatrix}2\sin\left(\beta_y^{+}+nt^*+n\Delta t_w\right)\cos\left(nt^*+n\Delta t_w\right)+\\+2\sin\left(\beta_y^{+}+n\frac{5}{4}t^*+n\Delta t_w\right)\cos\left(nt^*+n\Delta t_w\right)+\\+4\sin\left(\beta_y^{+}+n\frac{5}{4}t^*+n\Delta t_w\right)\cos\left(n\frac{t^*}{2}\right)\end{pmatrix} \tag{17}$$

where the $\beta_{y_i}^{+}$ become a common β_y^{+}, given the nature of the firings of same duration in the profile of Eq. (13). Eq. (17) still provides little information about what to expect at the end of the firing sequence. Since t^* is determined in Eq. (15), as well as the β_y^{+}, through Eq. (12c), the only free variable in Eq. (17) is the wait time between the series of firings Δt_w. One observation to be made is that the term under the square root is never expected to be zero, since it would imply firing with

Table 1
Initial Orbital parameters for S/C and desired trajectory for Leader-Follower case, plus general data for simulations.

Initial orbital parameter	Chief	Deputy
Semi-major axis a	6778.1 km	6778.1 km
Eccentricity e	0	0
Inclination i_{orb}	97.9908 deg	97.9908 deg
Right ascension of the ascending node (RAAN) Ω	261.621 deg	261.621 deg
Argument of perigee ω_p	30 deg	30 deg
Polar angle υ	27.216 deg	27.18 deg
Additional parameters used for the simulations		
$R_{\text{Earth}} = 6378.1363$ km $\quad \mu = 398,600.4418$ km^3/s^2		

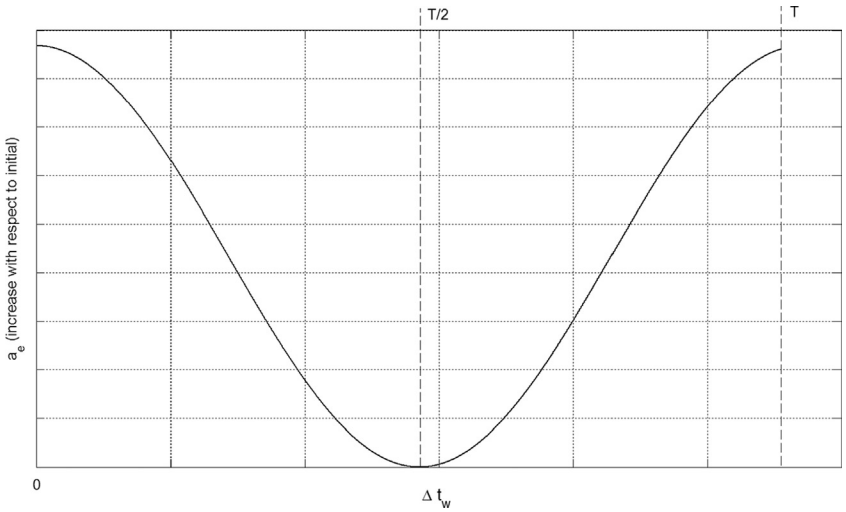

Fig. 5. Example of a_e vs. Δt_w for leader follower initial condition. *Note*: The above graph is obtained using the numerical data of Table 1, showing the min and max points.

no duration. For this reason we need only focus on the parenthesis term. The derivative of this parenthesis term with respect to Δt_w yields

$$2\ \cos\left(\beta_y^+ + n\Delta t_w + \tfrac{3}{4}nt^*\right) + 2\ \cos\left(\beta_y^+ + n\Delta t_w + \tfrac{7}{4}nt^*\right) +$$

$$+2\ \cos\left(\beta_y^+ + 2n\Delta t_w + 2nt^*\right) + 2\ \cos\left(\beta_y^+ + 2n\Delta t_w + \frac{9}{4}nt^*\right) \tag{18}$$

This shows that at the most four values for Δt_w can represent a minimum/maximum for Eq. (17), within an orbital period ($0 \le \Delta t_w \le T$). In fact, such a derivative is composed of four cosine functions, all shifted by different phases.

The locations of these minimum/maximum points change from case to case, depending on the values of β_y^+ and t^*. Despite the impracticability of solving Eq. (12a) in terms of Δt_w, even when simplified with the input-shaping profile, the derivative information allows us to predict the type of function we should expect, and, in addition, Eq. (17) clearly shows a

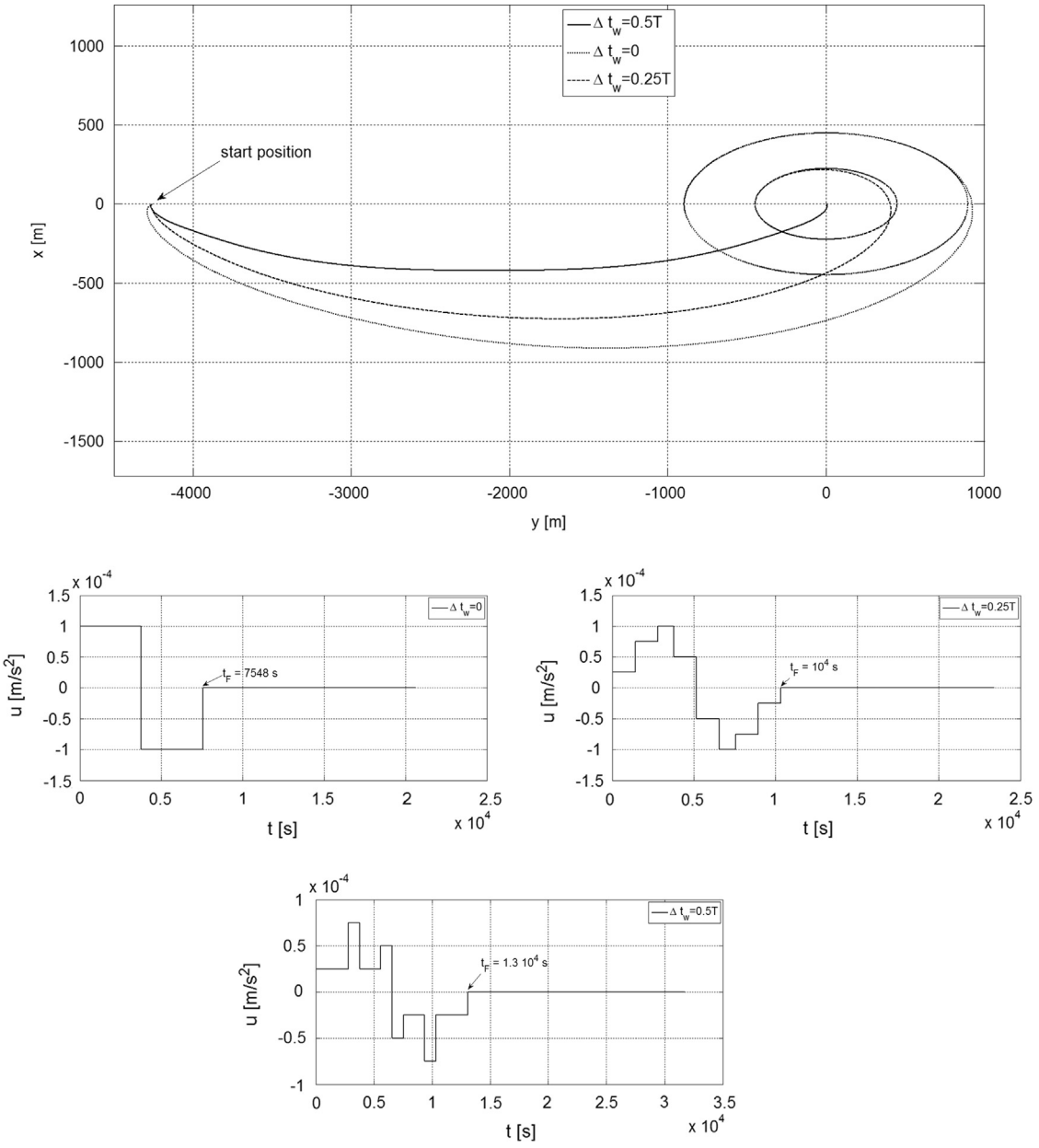

Fig. 6. Rendezvous with chief starting from an initial relative point. Top: (1) Δt_w=0.5 T, exact rendezvous with chief; (2) Δt_w=0, obtaining the maximum a_e for the final equilibrium orbit around the chief; (3) Δt_w=0.25 T, obtaining an intermediate value of a_e for the final equilibrium relative orbit around the chief. Bottom 3 plots: control profiles.

content in frequency, when using Δt_w as independent variable, not exceeding $2n$. The Nyquist–Shannon sampling theorem Ref. [21] enables capturing the nature of the function representing a_e when input-shaping is applied, and $\Delta t_w$is the independent variable, by computing Eq. (12a) only at Δt points spaced by a $1/4n$ distance, that is, theoretically 8π (i.e. 25 or more) points total in one orbital period time frame. A desired a_e value can be then interpolated using these required values (e.g. using splines), or more points, for increased accuracy purposes, posing no computational issues.

Depending on the initial conditions, the extrema for the a_e value can be four or less, and located at different Δt_w values between 0 and the orbital period T, as shown later on. In all cases there are special values of Δt_w that zero out the increase in a_e, that is, there are no oscillation size increases due to performing the maneuver.

It should be noted that for the other term under the radical in Eq. (12a), an identical expression can be found, the only difference being that the sine function in Eq. (16) would be replaced by a cosine function. Thus, the analysis of this term would be quite similar to that above.

5. Sample numerical simulations

In the following numerical simulations we assume a chief satellite located at the origin of the LVLH frame, and that we are maneuvering a deputy satellite. The chief represents the target trajectory for the different types of maneuvers here presented, i.e. we set up rendezvous problems. More generally, such a target trajectory can be a virtual satellite, and can be located anywhere such that the chief and deputy orbital periods are equal. The following numerical simulations are obtained using the results presented earlier. One example of closed-loop control is also presented where the ROEs-based guidance is recomputed when reaching its final time, for three times. This improves accuracy when the proposed guidance is used with the more realistic nonlinear Keplerian dynamics plus J2, and provides a proof for potential flight implementation. For all the simulations the control value $c=2\times10^{-5}$ m/s^2 is used, representing a low-thrust thruster. In principle, any c value can be chosen, representing the thrust available on the spacecraft.

The initial orbital parameters of Table 1 are used to generate the trajectories for the first simulation, representing an initial condition of leader-follower. Note that the initial orbital parameters are first converted to Cartesian position and velocity in an Earth centered inertial frame, then translated kinematically into the LVLH frame, and finally forced to match a leader follower initial condition for the linear equations, i.e. cancelling any residual relative velocity and x displacement.

Table 2
Initial Orbital parameters for S/C and desired trajectory for equilibrium-to-equilibrium case.

Orbital parameter	Chief	Deputy
Semi-major axis a	6778.1 km	6778.1 km
Eccentricity e	0	0.0001
Inclination i_{orb}	97.9908 deg	97.9908 deg
Right ascension of the ascending node (RAAN) Ω	261.621 deg	261.621 deg
Argument of perigee ω_p	30 deg	30 deg
Polar angle υ	27.216 deg	27.18 deg

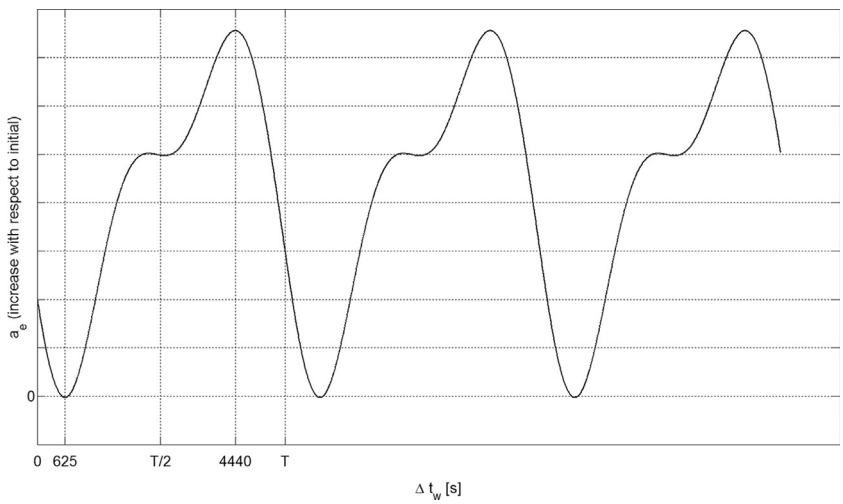

Fig. 7. Example of a_e vs. Δt_w for equilibrium relative orbit initial condition. *Note*: The above graph is obtained using the numerical data of Table 2, showing the min and max points.

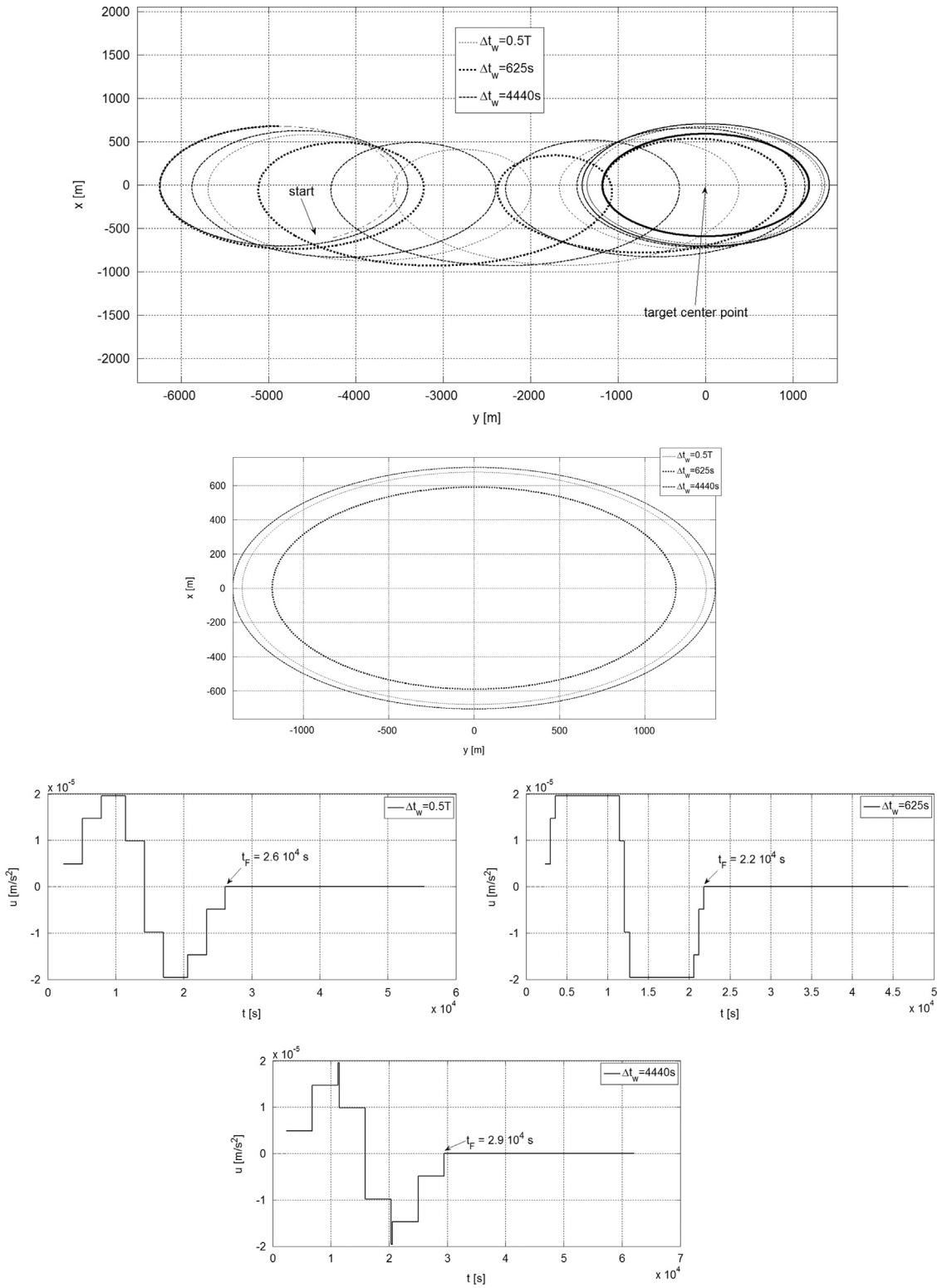

Fig. 8. Rendezvous with chief starting from an initial relative equilibrium orbit. Top: (1) $\Delta t_w = 0.5\,\mathrm{T}$, obtaining an intermediate a_e (between initial and maximum achievable) on final relative orbit; (2) $\Delta t_w = 625$ s, obtaining the minimum a_e for the final equilibrium orbit around the chief; (3) $\Delta t_w = 4440$ s, obtaining the maximum of a_e for the final equilibrium relative orbit around the chief. Center: zoom of the final relative orbits. Bottom 3 plots: control profiles.

Three different final conditions are chosen for this simulation, one being exact rendezvous and two cases where the final motion is a relative closed orbit around the chief. For these cases, the variation of final a_e as function of Δt_w reduces to a simple cosine function, with maximum at $\Delta t_w=0$ and one orbital period, and no increase at one-half orbital period (see Fig. 5). Fig. 6 shows the resulting trajectories applying input-shaping, as well as the control profiles as dictated by Eqs. (13) and (15). Note that in each case, the motion is simulated beyond t_F (t_F is indicated on the control plots for each case in Fig. 6). This is done to illustrate clearly the final trajectory achieved in each case.

Table 2 introduces a small eccentricity in the deputy initial orbital parameters, thus creating an initial motion which is a relative closed orbit whose center is offset from the chief by the same amount as the leader-follower separation in the previous cases. Note that the initial orbital parameters are first converted to Cartesian coordinates in an Earth centered inertial frame, then translated kinematically into the LVLH frame, and finally forced to match an equilibrium motion initial condition for the linear equations, i.e. imposing the condition $\dot{y}_0 = -2\omega x_0$ Ref. [17]. For these scenarios, the final a_e function is more complicated than before. Fig. 7 indicates that $\Delta t_w=625$ s yields no change in a_e, $\Delta t_w=4440$ s yields the maximum

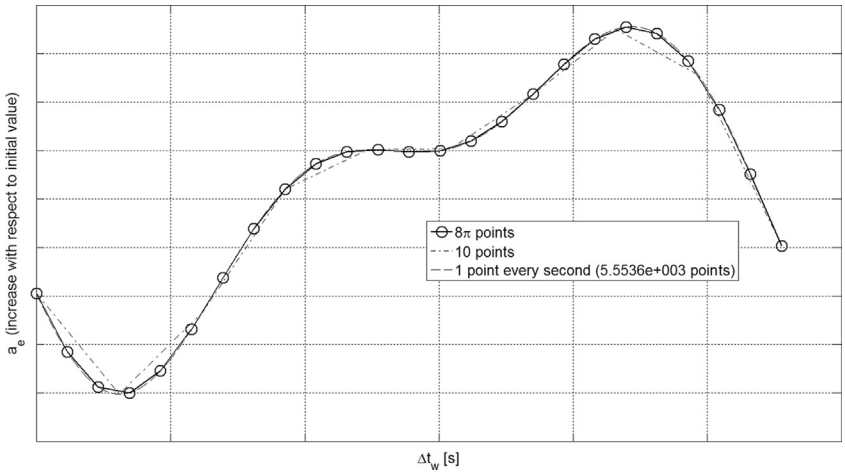

Fig. 9. Graphical demonstration of the number of points needed to represent the $a_e(\Delta t_w)$ function.

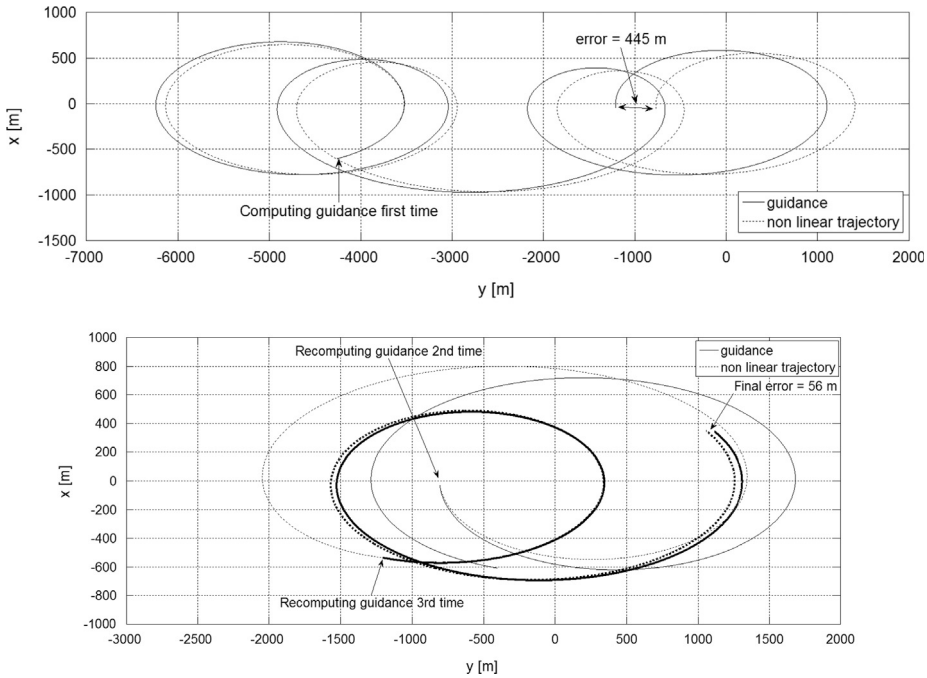

Fig. 10. Example of closed-loop guidance solving the ROEs input-shaping-based solution iteratively, with $\Delta t_w=0$. (Top) first iteration, (bottom) and two more iterations.

final value of a_e, and $\Delta t_w = 0.5$ T yields an intermediate final value of a_e. These results are shown in Fig. 8, including both the x–y trajectories and the control profiles. Note again that the motion is simulated beyond t_F in each case to illustrate the final trajectory achieved.

All the maneuvers can be computed analytically, from Eq. (15) and the earlier observations on the function $a_e(\Delta t_w)$. The only numerical operation required to design such maneuvers consists of reconstructing $a_e(\Delta t_w)$ by means of computing Eq. (12a) at a few points, and interpolating when a desired change in a_e is given, to solve for the corresponding Δt_w. This provides a powerful tool to design guidance trajectories onboard spacecraft with limited computing capabilities.

Fig. 9 compares three reconstructions of the $a_e(\Delta t_w)$ function: the one using the necessary 8π points, minimally differing from the more accurate line obtained with a sample time of 1 s. The third line shows how less than 8π points (10 in the example) lead to a poor reconstruction of the curve. The circles indicate the (Δt_w, a_e) points required for the curve reconstruction. Once those are stored in a table, a desired a_e value leads to the corresponding Δt_w by linearly interpolating between the two closest a_e points.

Fig. 10 shows an example where the ROEs input-shaping-based solution for equilibrium relative orbit to equilibrium relative orbit is solved iteratively, to obtain a closed-loop simulation considering a more realistic nonlinear dynamics for the relative motion. The solution of Eq. (15) with $\Delta t_w = 0$ is recomputed three times, at the end of each sequence. The maneuver is intended to move the center of the already excited equilibrium relative orbit, starting from the same initial conditions of the simulation presented in Fig. 8 and Table 2. The nonlinear relative motion is simulated using Keplerian dynamics plus J2 for each satellite, and then projecting the relative position and velocity vectors in the LVLH frame. Fig. 10 shows that the first iteration achieves a position magnitude error of 445 m between the analytically (re)generated guidance and the nonlinear trajectory. This error actually increases in the second iteration, but then decreases to a very acceptable 56 m in the third iterationa decrease in the error between the analytically (re)generated guidance and the nonlinear trajectory, starting from 445 m and ending at 56 m after 3 iterations. Particularly, the bolded lines in the bottom plot of Fig. 10 highlight the guidance trajectory and corresponding nonlinear trajectory for the third iteration, showing a close match between the two motions for the entire duration of the trajectory. In performing this simulation, it was noted that the accuracy with which the nonlinear trajectory achieved the desired final closed relative orbit was consistent with the position magnitude error described above. That is, the error between the actual final ROEs achieved by the nonlinear trajectory and the desired final ROEs *increased* from the first to the second iteration, and *decreased* from the second to the third iteration. In a real mission scenario, mid-course corrections may be advised, to maintain a lower tracking error.

More generally, the new equations providing the ROEs' time evolution in analytical form, when continuous, on-off thrust is applied, hold the potential for testing and designing new open loop control sequences. They could also provide analytical initial guesses for numerical optimization of the guidance.

6. Conclusion

This paper presents the general analytical solutions for spacecraft relative orbit control, when on/off continuous thrusters are used, employing relative orbit elements instead of classical Cartesian coordinates to represent the relative dynamics. Relative orbit elements are a powerful tool to visualize geometrical aspects of spacecraft relative motion. A thrust profile based on the input-shaping technique is used to validate the obtained formulas. The analytical solutions for exact re-phasing or rendezvous using input-shaping are provided, along with the expressions and procedures to control the size of the final relative orbit around the target trajectory or chief satellite. Sample numerical simulations show the type of maneuvers achievable using the ROE formulas and input-shaping control profiles, namely, re-phasing or rendezvous maneuvers with along-track control only.

The new analytical solutions in terms of ROEs, and particularly their simplifications, as done in the input-shaping case, can be implemented onboard small spacecraft with limited computing capabilities, allowing them to autonomously compute guidance trajectories of several kinds. In addition, optimization routines running on the ground could be envisioned, using as initial guess the here proposed formulas. The ROEs analytical solutions, simplified when applying the problem specific constraints (such as fixed value for the thrust, duration of thrust, etc.) can be used as the core for fast direct methods of numerical optimization, the advantage being the a-priori satisfaction of the constraints provided by the nature of the solutions.

Acknowledgments

The first author wishes to acknowledge the American Society for Engineering Education (ASEE) and the Air Force Research Laboratory (AFRL), Space Vehicles Directorate, Kirtland AFB, NM, for the opportunity to participate in the 2012 Air Force Summer Faculty Fellowship Program. The initial results were obtained during summer 2012 at AFRL.

References

[1] P. Thakker, W. Shiroma, Emergence of pico- and nanosatellites for atmospheric research and technology testing, Prog. Astronaut. Aeronaut. AIAA 234 (2010) 391. http://dx.doi.org/10.2514/4.867699, (September 15).
[2] J.D. Burges, M.J. Hall, E.G. Lightsey, Evaluation of a dual-fluid cold-gas thruster concept, Int. J. Mech. Aerosp. Eng. 6 (2012) 232–237.

[3] C.L. LEONARD, W.M. HOLLISTER, E.V. BERGMANN., Orbital formationkeeping with differential drag, J. Guid. Control Dynam. 12 (1) (1989) 108–113, http://dx.doi.org/10.2514/3.20374.
[4] Phil Palmer, Reachability and optimal phasing for reconfiguration in near-circular orbit formations, J. Guid. Control Dyn. 30 (5) (2007) 1542–1546, http://dx.doi.org/10.2514/1.28644.
[5] R. Bevilacqua, M. Romano, F. Curti, Decoupled-natural-dynamics model for the relative motion of two spacecraft without and with J2 perturbation, Nonlinear Dyn. Syst. Theory 10 (1) (2010) 11–20.
[6] Klaus Schilling Mauricio Guelman, Danna Linn Barnett, Formation flight line of sight guidance, Acta Astronaut. 71 (2012) 163–169, http://dx.doi.org/10.1016/j.actaastro.2011.08.004. (0094–5765).
[7] A. Banerjee, N. Pedreiro, W. Singhose, Vibration reduction for flexible spacecraft following momentum dumping with/without slewing, AIAA J. Guid. Control Dyn. 24 (2001) 417–428.
[8] Craig F. Cutforth, Lucy Y. Pao, Adaptive input shaping for maneuvering flexible structures, Automatica 40 (2004) 685–693, http://dx.doi.org/10.1016/j.automatica.2003.11.013.
[9] Lucy Y. Pao, Analysis of the frequency, damping, and total insensitivities of input shaping designs, AIAA J. Guid. Control Dyn. 20 (5) (1997).
[10] Matthew D. Baumgart, Lucy Y. Pao, Discrete time-optimal command shaping, Automatica 43 (2007) 1403–1409, http://dx.doi.org/10.1016/j.automatica.2007.01.003.
[11] Mark A. Lau, Lucy Y. Pao, Input shaping and time-optimal control of flexible structures, Automatica 39 (2003) 893–900, http://dx.doi.org/10.1016/S0005-1098(03)00024-4.
[12] Lucy Y. Pao, Craig F. Cutforth, On frequency-domain and time-domain input shaping for multi-mode flexible structures, J. Dyn. Syst. Meas. Contr. 125 (2003) 494–497, http://dx.doi.org/10.1115/1.1591808. (SEPTEMBER).
[13] Lucy Y. Pao, Mark A. Lau, Expected residual vibration of traditional and hybrid input shaping designs, AIAA J. Guid. Control Dyn. 22 (1) (1998) 162–165.
[14] M. Romano, B.N. Agrawal, F. Bernelli-Zazzera, Experiments on command shaping control of a manipulator with flexible links, AIAA J. Guid. Control Dyn. 25 (2) (2002) 232–239.
[15] ⟨http://www.riccardobevilacqua.com/links.html⟩.
[16] G.W. Hill, Researches in the lunar theory, Am. J. Math. 1 (1878) 5–26.
[17] W.H. Clohessy, R.S. Wiltshire, Terminal guidance system for satellite rendezvous, J. Aerosp. Sci. 27 (9) (1960) 653–658.
[18] T. Alan Lovell, Steven G. Tragesser, Guidance for relative motion of low earth orbit spacecraft based on relative orbit elements, AIAA Paper 2004-4988, AIAA/AAS Astrodynamics Specialist Conference and Exhibit, Providence, Rhode Island, 2004/08/16–2004/08/19.
[19] Riccardo Bevilacqua, Analytical guidance solutions for spacecraft planar rephasing via input shaping, J. Guid. Control Dyn. (2014), http://dx.doi.org/10.2514/1.G000008. (Published online at [retrieved February 20, 2014])⟨http://arc.aiaa.org/doi/abs/10.2514/1.G000008⟩.
[20] ⟨http://www.riccardobevilacqua.com/multimedia.html⟩.
[21] C.E. Shannon, Communication in the presence of noise, Proc. Inst. Radio Eng. 37 (1) (1998) 10–21. (Jan. 1949. Reprint as classic paper in: Proc. IEEE, vol. 86, no. 2, (Feb.).

Dr. Riccardo Bevilacqua is an Assistant Professor of the Mechanical, Aerospace, and Nuclear Engineering Department, at Rensselaer Polytechnic Institute. He holds a M. Sc. in Aerospace Engineering (2002), and a Ph.D. in Applied Mathematics (2007), both earned at the University of Rome, "Sapienza", Italy. He was a US National Research Council Post-Doctoral Fellow from 2007 to 2010, before joining RPI. He also worked as project engineer in Mission Analysis at Grupo Mecanica del Vuelo, in Madrid, Spain, during 2003. Dr. Bevilacqua's research interests focus on Guidance, Navigation, and Control of multiple spacecraft systems and multiple robot systems.

Dr. Thomas Alan Lovell is a Research Aerospace Engineer in the Space Vehicles Directorate of the Air Force Research Laboratory. He received his Ph.D. from Auburn University in Aerospace Engineering in 2001. He has authored or co-authored over 60 conference papers and a dozen journal articles. He is a Senior Member of AAS, and an Associate Fellow of AIAA. He serves on the AIAA Astrodynamics Technical Committee. He is also an Associate Editor for the AIAA Journal of Guidance, Control, and Dynamics. His research interests include astrodynamics, orbit determination, trajectory optimization, and feedback control design.